


Cite this: *Anal. Methods*, 2026, 18, 3172

# Magnetic chitosan/ZIF-L/KCDs granular-leaf hybrid nanocomposite for magnetic dispersive $\mu$ solid phase extraction of mycotoxins from ziziphus jujuba, nuts and grains

Mahboube Shirani,<sup>\*a</sup> Qamar Salamat,<sup>b</sup> Mohammadjavad Jahanshahi,<sup>a</sup> Soheila Sepahi<sup>c</sup> and Mustafa Soylak <sup>\*bdef</sup>

In this study, a novel magnetic chitosan/zeolitic imidazolate frameworks-L/kiwi peel-derived carbon dots (MCS/ZIF-L/KCDs) granular-leaf hybrid nanocomposite was synthesized and used for magnetic dispersive  $\mu$ solid-phase extraction (MD- $\mu$ SPE) of aflatoxins B1, B2, G1, and G2, and the extracts were analyzed by high-performance liquid chromatography with fluorescence detection (HPLC-FLD). The sorbent was characterized using Fourier-transform infrared spectroscopy, X-ray diffraction, scanning electron microscopy, and energy-dispersive X-ray spectroscopy. The influential parameters were optimized, and under optimum conditions, the developed method showed excellent analytical performance with limits of detection (LOD) of 0.002–0.003  $\mu\text{g kg}^{-1}$ , limits of quantification (LOQ) of 0.007–0.009  $\mu\text{g kg}^{-1}$ , and linear dynamic ranges (LDR) of 0.01–750 and 0.01–1000  $\mu\text{g kg}^{-1}$ , depending on the analyte and matrix. The relative recoveries (%) of 91.0–99.4, and the intra-day ( $n = 6$ ) and inter-day (5 days,  $n = 3$ ) precisions at  $\leq 3.5\%$  and  $\leq 3.0\%$ , were acquired, respectively, which confirmed satisfactory capability, reproducibility, and repeatability. The proposed method presented good compliance with green analytical chemistry rules.

Received 4th February 2026  
Accepted 15th March 2026

DOI: 10.1039/d6ay00202a

rsc.li/methods

## 1. Introduction

Aflatoxins are a class of dangerous mycotoxins engendered by certain types of *Aspergillus* fungi, especially *Aspergillus flavus* and *Aspergillus parasiticus*.<sup>1</sup> These toxins are primarily found in agricultural products such as cereals, seeds, and nuts, and they seriously affect human and animal health.<sup>2</sup> Aflatoxins B and G are among the most important and common types of aflatoxins. Aflatoxin B1 is recognized as the most potent and carcinogenic kind, typically found in grains such as corn, wheat, and rice.<sup>3</sup> Similarly, aflatoxin G1 is also hazardous and is produced under similar conditions. These toxins can be transmitted through the food chain to humans, posing significant risks to public health,

including liver diseases, cancer, and immune disorders.<sup>4</sup> Controlling aflatoxin contamination in cereals is a major challenge for the agricultural and food industries.<sup>5</sup> Environmental conditions such as humidity and temperature can influence the production of these toxins; therefore, careful monitoring and appropriate management during the cultivation, harvesting, and storage of grains are essential.<sup>6</sup> Additionally, regulatory agencies have established maximum allowable limits for aflatoxins to protect consumer health.<sup>7</sup> The following decades saw the development of detection methods such as HPLC and GC, with organizations like the FDA and WHO establishing safety standards in the 1970s.<sup>8</sup> Today, monitoring of aflatoxins in food products has become a global focus due to increased trade, with ongoing research aimed at reducing health risks associated with these toxins.<sup>9</sup> Various analytical techniques have been applied. However, owing to the very low concentration of aflatoxins in food samples, application of a susceptible analytical method is essential, which requires the combination of an intense sample treatment method and a sensitive analytical technique.<sup>10</sup> Magnetic solid-phase extraction (MSPE) is an effective method for extracting aflatoxins B and G from various samples.<sup>11</sup> This process involves preparing magnetic adsorbents, often iron oxide particles that are coated to enhance selectivity.<sup>12</sup> Samples such as grains or dairy products are collected and processed to optimize adsorption conditions.

<sup>a</sup>Department of Chemistry, Faculty of Science, University of Jiroft, P. O. Box 7867161167, Jiroft, Iran. E-mail: m.shirani@ujiroft.ac.ir; Fax: +98-3443347065; Tel: +98-3443347061

<sup>b</sup>Department of Chemistry, Faculty of Sciences, Erciyes University, Kayseri, Turkey. E-mail: msoylak@gmail.com; soylak@erciyes.edu.tr

<sup>c</sup>Laboratories of Food and Drug Control, Vice Chancellery for Food and Drug, Isfahan University of Medical Sciences, Isfahan, Iran

<sup>d</sup>Technology Research and Application Center (ERU-TAUM), Erciyes University, 38039 Kayseri, Turkey

<sup>e</sup>Turkish Academy of Sciences (TUBA), Çankaya, Ankara, Turkey

<sup>f</sup>Nano Bioanalytical Chemistry Center (NBACC), Khazar University, Mahsati Str 41, Baku, AZ-1096, Azerbaijan



After mixing the sample with the adsorbent, a magnet is used to separate the adsorbent containing aflatoxins.<sup>13</sup> The adsorbent is then washed, and aflatoxins are eluted with suitable solvents before being analyzed using atomic/emission spectrometry, high-performance liquid chromatography (HPLC),<sup>14</sup> or gas chromatography (GC). MSPE offers advantages such as high sensitivity, reduced extraction time, and lower contamination risk, but requires specialized equipment and may incur higher initial costs. Overall, it is a valuable technique for assessing food safety and quality. Quantum dots<sup>15</sup> and zeolitic imidazolate frameworks (ZIFs)<sup>16</sup> are effective materials used for extraction and separation processes. Quantum dots are semiconductor nanoparticles known for their high sensitivity, stability, and tunable properties, allowing them to selectively identify target compounds such as toxins and drugs.<sup>17</sup> ZIFs, which are constructed as porous materials, provide large pores, selectivity, and thermal stability, making them suitable for gas separation, water purification, and nutrient extraction.<sup>18</sup> Combining quantum dots with ZIFs enhances sensitivity and opens new applications in environmental sensing and drug detection. The synthesis of these materials involves precise control over conditions and components, including metal salts, ligands, and precursors of quantum dots.<sup>19</sup> Overall, these materials promise advancements in materials science and analytical chemistry. The synthesis of zeolitic imidazolate frameworks (ZIFs) with quantum dots involves several precise steps. The main raw materials include metal salts (e.g.,  $\text{Zn}(\text{NO}_3)_2$ ), ligands (e.g., 2-methylimidazole), quantum dot precursors (such as CdSe), and solvents. This process includes the synthesis of quantum dots by dissolving precursors, heating, cooling, and washing. Subsequently, ZIFs are formed by mixing metal and ligand solutions with quantum dots, followed by incubation at controlled temperatures. The final stages involve filtering, washing, and drying the product. Using zinc imidazolate frameworks (ZIFs) as a quantum dot adsorbent for the adsorption of aflatoxins B and G presents a novel approach in analytical chemistry, leveraging their porous structure and strong adsorption features. In recent years, different MOF- and ZIF-based materials have been investigated for aflatoxin extraction, removal, and detection. In addition, related chitosan/MOF composites and MOF/carbon-dot systems have also been reported in the literature for aflatoxin-related applications.<sup>20–23</sup> Therefore, the novelty of the present study is not the general use of magnetic MOF/ZIF sorbents alone. Rather, this work introduces a hierarchical MCS/ZIF-L/KCDs nanocomposite in which magnetic chitosan provides magnetic separability and a biopolymeric support, ZIF-L, supplies a leaf-like porous framework with abundant accessible adsorption sites, and KCDs enrich the surface with additional oxygen-containing functional groups and structural heterogeneity. To the best of our knowledge, this specific MCS/ZIF-L/KCDs ternary sorbent has not been previously applied to the simultaneous magnetic dispersive micro-solid phase extraction of aflatoxins B1, B2, G1, and G2 from ziziphus jujube, wheat, corn, white rice, pistachio, and walnut samples before HPLC-FLD analysis.

## 2. Experimental

### 2.1. Chemicals

Aflatoxins B1, B2, G1, and G2 standards were purchased from Sigma Chemical Company (St. Louis, MO, USA). A working standard solution ( $10 \mu\text{g L}^{-1}$ ) was prepared by serial dilution in deionized water. Phosphate Buffered Saline (PBS) tablets (pH 7.4) were obtained from Sigma-Aldrich (USA). High-performance liquid chromatography (HPLC) grade solvents, including methanol, acetonitrile, acetone, and ethyl acetate, were purchased from Merck (Germany). For the synthesis of the nanocomposites, chitosan (low molecular weight), iron(III) chloride hexahydrate ( $\text{FeCl}_3 \cdot 6\text{H}_2\text{O}$ ), ammonium acetate ( $\text{NH}_4\text{Ac}$ ), and sodium citrate tribasic dihydrate ( $\text{C}_6\text{H}_5\text{Na}_3\text{O}_7 \cdot 2\text{H}_2\text{O}$ ) were used as precursors for the preparation of magnetic chitosan nanospheres (MCS) and were purchased from Sigma-Aldrich (Germany). Ethylene glycol was used as the reaction solvent for the MCS synthesis. Zinc nitrate hexahydrate ( $\text{Zn}(\text{NO}_3)_2 \cdot 6\text{H}_2\text{O}$ ) and 2-methylimidazole (2-MIM), used for the growth of ZIF-L nanosheets, were also obtained from Sigma-Aldrich. Methanol was used as the dispersion medium during the synthesis of MCS/ZIF-L.

To prepare kiwi peel-derived carbon dots (KCDs), fresh kiwi fruit was purchased from a local market in Isfahan, Iran. Ethanol and deionized water (1:1, v/v) were used as the hydrothermal solvent for KCD synthesis. Syringe filters (0.2  $\mu\text{m}$  pore size) used for the purification of the KCD solution were purchased from Sartorius (Germany).

### 2.2. Instrumentation

Analytical HPLC (Dinox, USA) with an autosampler (ASI-100 Dinox, USA), quaternary pump (P680A, USA), fluorescence detector (model 170U, Dinox, USA), and C18 column (10 cm length and 4.6 mm inner diameter ODS2 column), equipped with a Kobra cell, was used for chromatographic analysis of aflatoxins B1, B2, G1, and G2. The mixture of MeOH : H<sub>2</sub>O : ACN (400 : 600 : 60 v/v) with potassium bromide (0.0131 g), and nitric acid (383  $\mu\text{L}$ ) was utilized as an isocratic mobile phase. The column temperature and the mobile phase flow rate were set at 25 °C and 1.2 mL min<sup>-1</sup>, respectively. The detector was set at the emission wavelength of 440 nm and the excitation wavelength of 360 nm. Fourier transform infrared (FT-IR) spectroscopy (PerkinElmer Range 400 spectrometer, Waltham, MA, USA) was used to identify the functional groups on the surface of the sorbent. An instrument with a step size of 0.262606 from XRD-BRUKER AXS D8 ADVANCE, Türkiye, was used for X-ray diffraction (XRD). Surface morphology was examined using a field-emission scanning electron microscope (FE-SEM, ZEISS Crossbeam 550, Germany).

### 2.3. Sample preparation

Ziziphus jujube, wheat, corn, white rice, pistachio, and walnut were bought from a local grocery store in Isfahan, Isfahan Province, Iran. To prepare the real samples, the following procedure was carried out:



5.0 g of each sample (ziziphus jujube powder, wheat, corn, and white rice) was weighed and transferred to a 50 mL Falcon tube, then 0.5 g sodium chloride, 24 mL methanol, and 6 mL HPLC water were added, and the mixture was vortexed in the dark for 10 min. Then, it was centrifuged at 6500 rpm for 10 min. 3 mL of the upper phase was passed through a glass filter (0.1 micron). The filtrate was diluted to 25 mL with PBS solution.

For the pistachio and walnut samples, the slurry should first be prepared. 5 g of each sample was added to a 50 mL Erlenmeyer flask, and 0.25 g sodium chloride, 15 mL methanol, and 5 mL *n*-hexane were added, and the mixture was vortexed in the dark for 5 min. The mixture was centrifuged, and the 2.5 mL upper phase was filtered through a glass filter and then diluted to 25 mL with PBS solution. The prepared solution for all samples was used for the analytical process.

#### 2.4. Synthesis procedure of MCS/ZIF-L/KCDs nanocomposites

**2.4.1. KCD preparation.** KCDs were synthesized through an environmentally friendly, single-step hydrothermal approach utilizing desiccated kiwi peel.<sup>24</sup> At the outset, fresh kiwi peels were thoroughly washed with tap water to remove adhering pulp residues and surface impurities, and then rinsed several times with deionized water to eliminate any remaining contaminants. The cleaned peels were subsequently dried in an oven at 60 °C until a constant weight was achieved and then ground into a fine powder. After that, 4 g of the dried biomass was dispersed in 60 mL of a water–ethanol mixture (1 : 1, v/v). The resulting suspension was vigorously stirred and subjected to hydrothermal treatment at 120 °C for 24 h. After cooling to room temperature, a yellow solution with a visible precipitate was obtained. The suspension was carefully decanted to separate the dark yellow insoluble precipitate, and the supernatant was filtered through a 0.2 µm syringe filter to obtain a clear yellow carbon dot solution.<sup>25</sup>

**2.4.2. Synthesis of MCS.** Nanospheres of MCS were manufactured using a solvothermal method, incorporating changes to previously documented procedures.<sup>26</sup> Initially, 100 mg of chitosan was dissolved in 100 mL of ethylene glycol while being mechanically stirred to achieve a homogeneous solution. A mixture of metal precursors comprising 2.4 g of FeCl<sub>3</sub>·6H<sub>2</sub>O (9.0 mmol), 1.39 g of NH<sub>4</sub>Ac (18 mmol), and 0.85 g of C<sub>6</sub>H<sub>9</sub>Na<sub>3</sub>O<sub>9</sub> (2.9 mmol) was gradually incorporated into the chitosan dispersion and manually agitated for 15 min to attain a homogeneous mixture. The obtained solution was placed in a Teflon-lined autoclave and made to undergo heat treatment at 190 °C for 16 hours. Upon natural cooling to ambient temperature, a black precipitate was generated, which was subsequently isolated and rinsed multiple times with ethanol and deionized water until the supernatant appeared clear. The washed product (MCS) was subsequently dried in an oven at 60 °C overnight and kept for future use.

**2.4.3. Synthesis of MCS/ZIF-L/KCDs granular-leaf hybrid nanocomposites.** To synthesize MCS/ZIF-L nanosheets, 0.5 g of the previously synthesized MCS was suspended in 40 mL of

methanol and stirred for 10 min. Following this, 2.2 g of 2-methylimidazole (2-MIM, 26.8 mmol) and 3.0 g of Zn(NO<sub>3</sub>)<sub>2</sub>·6H<sub>2</sub>O (3.35 mmol) were introduced to the suspension, which was then stirred for 4.0 hours. To facilitate the creation of ZIF-L nanosheets on the MCS surface, the reaction mixture was placed under static conditions for 12 hours. The MCS/ZIF-L composite (Product A) was obtained by magnetically isolating the product, washing it with methanol, and then vacuum-drying it for 12 hours at 60 °C.<sup>27</sup>

To synthesize the ternary nanocomposite of MCS/ZIF-L/KCDs, 0.5 g of the MCS/ZIF-L composite (Product A) was dispersed in 50 mL of a previously produced KCD solution. The mixture was mechanically stirred at room temperature for 24 hours to ensure uniform loading of KCDs onto the ZIF-L-modified MCS. The final product was extracted using a magnet, thoroughly purified with ethanol, and subjected to vacuum drying at 60 °C for 12 hours to produce the MCS/ZIF-L/KCDs nanocomposite.

#### 2.5. pH of the isoelectric point

The pH of the point of zero charge (pH<sub>PZC</sub>) represents the pH at which the net surface charge of a material is zero, meaning that the positive and negative charges on the sorbent surface are balanced. At this pH, the material exhibits minimal electrostatic interaction with surrounding species due to the absence of an overall surface charge. To determine the pH<sub>PZC</sub> of the MCS/ZIF-L/KCDs nanocomposite, 10 mL of 0.1 mol L<sup>-1</sup> sodium nitrate (NaNO<sub>3</sub>) solution was transferred into twelve Falcon tubes. The initial pH values were adjusted in the range of 1–12 using dilute HCl or NaOH solutions. Subsequently, 10 mg of the nanocomposite was added to each tube. The suspensions were shaken for 24 h to reach equilibrium. After equilibration, the final pH values were measured, and the difference between the initial and final pH values (ΔpH) was calculated. The ΔpH values were plotted against the initial pH, and the point where the curve crossed ΔpH = 0 was taken as the pH<sub>PZC</sub>. As shown in Fig. S1, the pH<sub>PZC</sub> of the MCS/ZIF-L/KCDs sorbent was found to be 7.3, indicating that the sorbent surface is nearly electrically neutral around physiological pH.

#### 2.6. Analytical procedure

A volume of 25 mL sample solution was transferred to a Falcon tube, and 30 mg of MCS/ZIF-L/KCDs was added to it and vortexed for 2 min to ensure efficient and rapid interaction between sorbent and analytes for preconcentration. Owing to the magnetic properties of the nanostructure sorbent, MCS/ZIF-L/KCDs were separated from the solution using an external magnet, and the upper phase was removed completely. 100 µL methanol was used to elute analytes from the sorbent after 90 s of sonication. Then, an external magnet was utilized to separate the magnetic nanocomposite. The methanol containing aflatoxins B1, B2, G1, and G2 were analyzed with HPLC-FLD. The calibration curves were acquired *via* the matrix matched method.



### 3. Results and discussion

#### 3.1. Characterization

The synthesis and structural evolution of the MCS, MCS/ZIF-L, and MCS/ZIF-L/KCDs composites were validated using various complementary characterization techniques. The analyses conducted using FTIR and XRD validated the chemical functionalities and crystalline changes at each stage of production. To investigate morphological evolution, SEM was utilized, uncovering unique surface topologies for each material. Furthermore, EDX was conducted to ascertain the elemental content and distribution within the composites, offering additional confirmation of the successful integration of each component (Fig. 1).

The FTIR spectra of MCS (Fig. 1(a)) exhibit a large band around  $\sim 3400\text{ cm}^{-1}$ , indicative of the O–H and N–H stretching

vibrations from chitosan and adsorbed water. Peaks detected at around  $2920$  and  $2850\text{ cm}^{-1}$  are ascribed to C–H stretching vibrations of aliphatic  $-\text{CH}_2$  groups. The peak at around  $1640\text{ cm}^{-1}$  is attributed to N–H bending or amide I, whereas the range of  $1100$ – $1030\text{ cm}^{-1}$  is associated with C–O–C stretching of glycosidic bonds. A prominent band at approximately  $570\text{ cm}^{-1}$  signifies Fe–O stretching, hence validating the integration of  $\text{Fe}_3\text{O}_4$  nanoparticles into the magnetic chitosan matrix. In the MCS/ZIF-L composite, distinct peaks at approximately  $1570$ – $1470\text{ cm}^{-1}$  belong to C=N and C=C stretching vibrations, whilst peaks at around  $1350$ – $900\text{ cm}^{-1}$  are ascribed to C–N stretching and aromatic C–H bending within the imidazole rings of ZIF-L. The Zn–N stretching vibration at around  $430$ – $450\text{ cm}^{-1}$  further corroborates the effective synthesis of the ZIF-L framework. The –OH/NH band exhibits a modest decrease in intensity and a shift, signifying coordination interactions

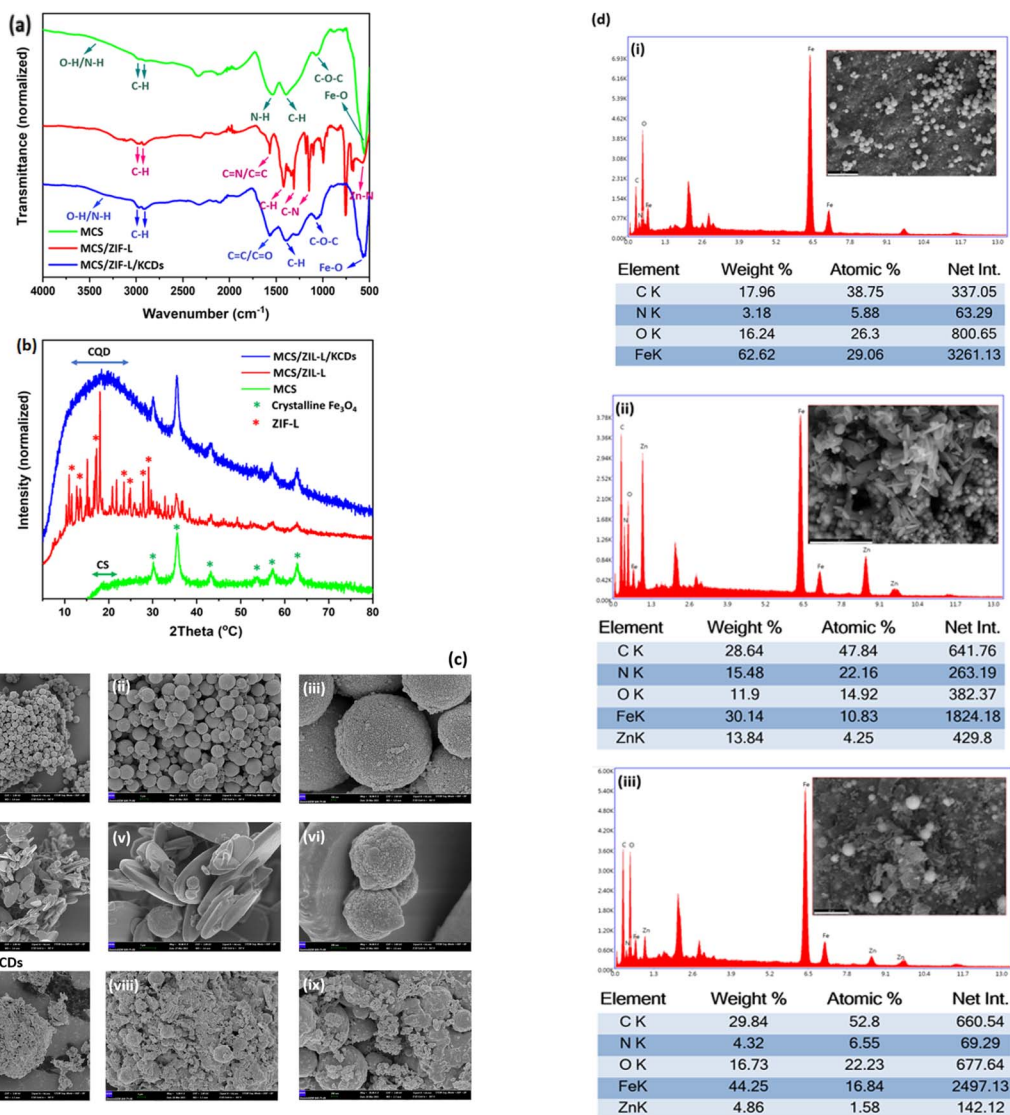


Fig. 1 (a) FTIR spectra of MCS, MCS/ZIF-L, and MCS/ZIF-L/KCDs nanocomposite, (b) XRD spectra of MCS, MCS/ZIF-L, and MCS/ZIF-L/KCDs nanocomposite, (c) SEM images of MCS (i–iii), MCS/ZIF-L (iv–vi), and MCS/ZIF-L/KCDs nanocomposite (vii–ix), (d) EDX spectra and the elemental composition of MCS (i), MCS/ZIF-L (ii), and MCS/ZIF-L/KCDs nanocomposite (iii).



between the functional groups of chitosan and the ZIF-L network.<sup>28</sup> The final MCS/ZIF-L/KCDs composite exhibits additional alterations. The substantial hydrogen bonding is indicated by the increased intensity of the broad -OH/NH band about  $\sim 3400\text{ cm}^{-1}$ , attributed to the surface -OH and -COOH groups of the KCDs. A novel peak at approximately  $1720\text{ cm}^{-1}$  is attributed to the C=O stretching vibration of carboxylic groups on KCDs, whereas bands at around  $1620$  and  $1400\text{ cm}^{-1}$  correspond to C=C and C-H bending, respectively. The C-O-C stretching reemerges at approximately  $1100\text{ cm}^{-1}$ , corroborating the existence of oxygenated groups from KCDs. The continued presence of Fe-O and Zn-N bands in the composite spectra confirms the structural integrity of the magnetic and ZIF-L components.<sup>29</sup>

Additional insights from XRD analysis (Fig. 1(b)) further support the sequential construction of the composite. The MCS pattern demonstrates broad diffraction at approximately  $20\text{--}25^\circ$  ( $2\theta$ ), indicating the amorphous nature of chitosan. In contrast, distinct peaks at approximately  $30.1^\circ$ ,  $35.4^\circ$ ,  $43.3^\circ$ ,  $53.7^\circ$ ,  $57.0^\circ$ , and  $62.6^\circ$  are associated with the (220), (311), (400), (422), (511), and (440) planes of crystalline  $\text{Fe}_3\text{O}_4$ , following JCPDS card no. 19-0629.<sup>30</sup> The inclusion of ZIF-L results in the emergence of distinct peaks at approximately  $11.7^\circ$ ,  $13.1^\circ$ ,  $17.0^\circ$ ,  $22.2^\circ$ ,  $24.6^\circ$ ,  $26.7^\circ$ , and  $29.9^\circ$ , which correspond to the unique diffraction pattern of ZIF-L. This confirms the effective crystallization of the ZIF-L structure on the MCS surface.<sup>28</sup> The resulting MCS/ZIF-L/KCDs composite exhibits a significant broadening of peaks and an overall reduction in intensity. The prominence of the hump in the  $\sim 20\text{--}30^\circ$  range is enhanced by the semi-crystalline or amorphous characteristics of KCDs. Although certain reflections from ZIF-L persist, their diminished intensity and minor displacements suggest structural distortion and obscuration by CDs.<sup>31</sup>

The SEM images (Fig. 1(c)) show that the pristine MCS (images i–iii) displays a consistent, spherical morphology, with particle sizes ranging from sub-micron to several microns in diameter. Images (i) and (ii) show spherical particles that are smooth and densely packed, suggesting effective dispersion of  $\text{Fe}_3\text{O}_4$  nanoparticles within the chitosan matrix. Higher magnification (image iii) reveals the fine, textured surfaces of individual microspheres, which could provide active sites for surface interactions. The spherical shape is consistent with literature reports of magnetically induced self-assembly of chitosan-based composites.<sup>32</sup> Upon the growth of the ZIF-L framework on the MCS surface (MCS/ZIF-L), significant morphological changes are observed. Images (iv) and (v) display the formation of leaf-like crystalline platelets, which are typical of ZIF-L's two-dimensional structure. These platelets are radially grown and appear densely anchored on the surface of the MCS spheres, creating a rough, flower-like composite architecture. The graph in (vi) demonstrates that the spherical MCS particles are visible beneath the ZIF-L layer, hence proving the successful occurrence of heterogeneous nucleation. This hierarchical structure is expected to enhance the surface area and active sites, hence improving adsorption or catalytic applications.<sup>33</sup> The addition of KCDs further alters the surface properties, as illustrated in images (vii) to (ix) (MCS/ZIF-L/KCDs).

The overall structure exhibits a rougher and more granular quality, with the leaf-like characteristics largely hidden beneath a chaotic, delicate layer. This coating is associated with KCD aggregates that enhance and potentially connect the ZIF-L platelets. The nanoscale granular features displayed by KCDs are visible in the high-magnification images (viii and ix), indicating successful deposition and surface functionalization. The KCDs demonstrate the ability to enhance conductivity, dispersibility, and the availability of functional groups on the composite surface.<sup>29</sup>

Regarding the SEM-EDX images (Fig. 1(d)), the spectrum of the MCS composite (image i) shows the presence of carbon (C), nitrogen (N), oxygen (O), and a prominent signal from iron (Fe). The increased Fe content (62.62 wt%) confirms the successful incorporation of  $\text{Fe}_3\text{O}_4$  nanoparticles into the chitosan matrix. The significant peaks of C (17.96 wt%) and O (16.24 wt%) arise from the chitosan backbone and the adsorbed functional groups, whereas N (3.18 wt%) signifies the presence of amine groups derived from deacetylated chitosan. The findings are consistent with established literature and confirm the effective synthesis of the MCS support, demonstrating magnetic characteristics. The elemental profile in the MCS/ZIF-L composite, as illustrated in image ii, undergoes significant alteration with the addition of ZIF-L to the MCS support. A significant increase in C (28.64 wt%) and N (15.48 wt%) is observed, both indicating the incorporation of the 2-MIM linker in the synthesis of ZIF. The appearance of Zn peaks (13.84 wt%) along with a reduction in Fe (30.14 wt%) indicates partial surface coverage of the MCS spheres by ZIF-L crystals. The Zn : Fe ratio supports the effective growth of ZIF-L onto the magnetic chitosan surface. The enhanced nitrogen content also confirms the introduction of nitrogen-rich imidazole groups, validating the formation of the ZIF framework. After the integration of KCDs, the EDX profile of the MCS/ZIF-L/KCDs composite (picture iii) indicates a notable increase in carbon content (29.84 wt%), aligning with the carbonaceous characteristics of KCDs. The Fe signal (44.25 wt%) persists, suggesting the preservation of the core magnetic structure. The Zn concentration (4.86 wt%) is significantly lower than that observed in the MCS/ZIF-L stage, likely due to inadequate coverage of the ZIF-L surface by KCDs. The identified contributions of O (16.73 wt%) and N (4.32 wt%) are attributed to oxygenated functional groups and nitrogen doping commonly observed in KCDs, along with residual contributions from chitosan and ZIF-L. The findings provide strong evidence for effective surface functionalization and composite synthesis.

### 3.2. Optimization of the MCS/ZIF-L/KCDs-MD- $\mu$ SPE process

The acidity and basicity of the analyte solution affect both the analyte's functional groups and the sorbent's functional groups. To this end, the pH of the solution was explored in the range of 3–10, and as shown in Fig. 2(a), the extraction recoveries enhanced from 3–7 and became constant from 7–8, and then decreased. Generally, aflatoxin structures can be hydrolyzed, and the lactonic ring may also be decomposed in strong basic or acidic media. Therefore, aflatoxins can be adsorbed on the surface of the MCS/ZIF-L/KCDs under neutral conditions *via*



hydrogen bonding,  $\pi$ - $\pi$ , and van der Waals interactions.<sup>34</sup> To set the pH of the solution, PBS buffer solution (pH = 7.4) was used. This optimum pH is also consistent with the experimentally determined  $\text{pH}_{\text{PZC}}$  value of 7.3 for the MCS/ZIF-L/KCDs sorbent (Fig. S1), suggesting favorable surface conditions for the extraction of aflatoxins under near-neutral conditions.

The amount of adsorbent determines the number of available active sites for analyte adsorption; therefore, increasing the sorbent dosage generally increases the number of accessible adsorption sites. The adsorbent dosage was studied in the range of 5–40 mg, and the optimum amount of 25 mg was attained (Fig. 2(b)).

Vortex time supplies a qualified period of time for the analytes to be adsorbed on the surface of the adsorbent. Therefore, vortex time was studied from 0.5 to 2.5 min, and as seen in Fig. 2(c), a time of 1.0 min was optimum and sufficient to allow analyte adsorption and separation.

The desorption solvent type plays an important role in the extraction efficiency. The desorption solvent should establish a strong interaction with the analyte to elute and desorb it from the sorbent. The effect of some desorption solvents, including methanol, acetone, acetonitrile, and ethyl acetate, was investigated. As shown by the results in Fig. 2(d), methanol could

desorb aflatoxins more efficiently, which may be due to the higher polarity of methanol (*via* hydrogen bonding interactions) and can interact with aflatoxins B1, B2, G1, and G2 as polar compounds. The order of polarity indexes of the desorption solvents of interest is methanol (6.6) > acetonitrile (6.2) > acetone (5.4), respectively, which confirms the obtained results.

Preconcentration factor (PF) is assessed as the ratio of sample solution volume to desorption solvent volume, and PF indicates the potency of the method to analyze trace/ultra-trace concentrations with higher sensitivity. The methanol volume was observed for the volumes of 50  $\mu\text{L}$  to 250  $\mu\text{L}$ , and as shown in Fig. 2(e), the extraction efficiencies for the four analytes increased from 50–100  $\mu\text{L}$  and then became constant. Hence, the volume of 100  $\mu\text{L}$  was selected as optimum for the rest of the studies, and the PF of 250 was achieved.

The desorption time is influential in providing an appropriate time for the desorption solvent to interact with the analyte and desorb it from the sorbent. The desorption time was explored from 30 s to 150 s, and as revealed in Fig. 2(f), the desorption time of 90 s was chosen for the rest of the studies.

The ionic strength of the solution is defined by adding a salt such as NaCl and is called the salting-in effect or salting-out. The concentration of NaCl was studied from 0 to 10% (w/v),

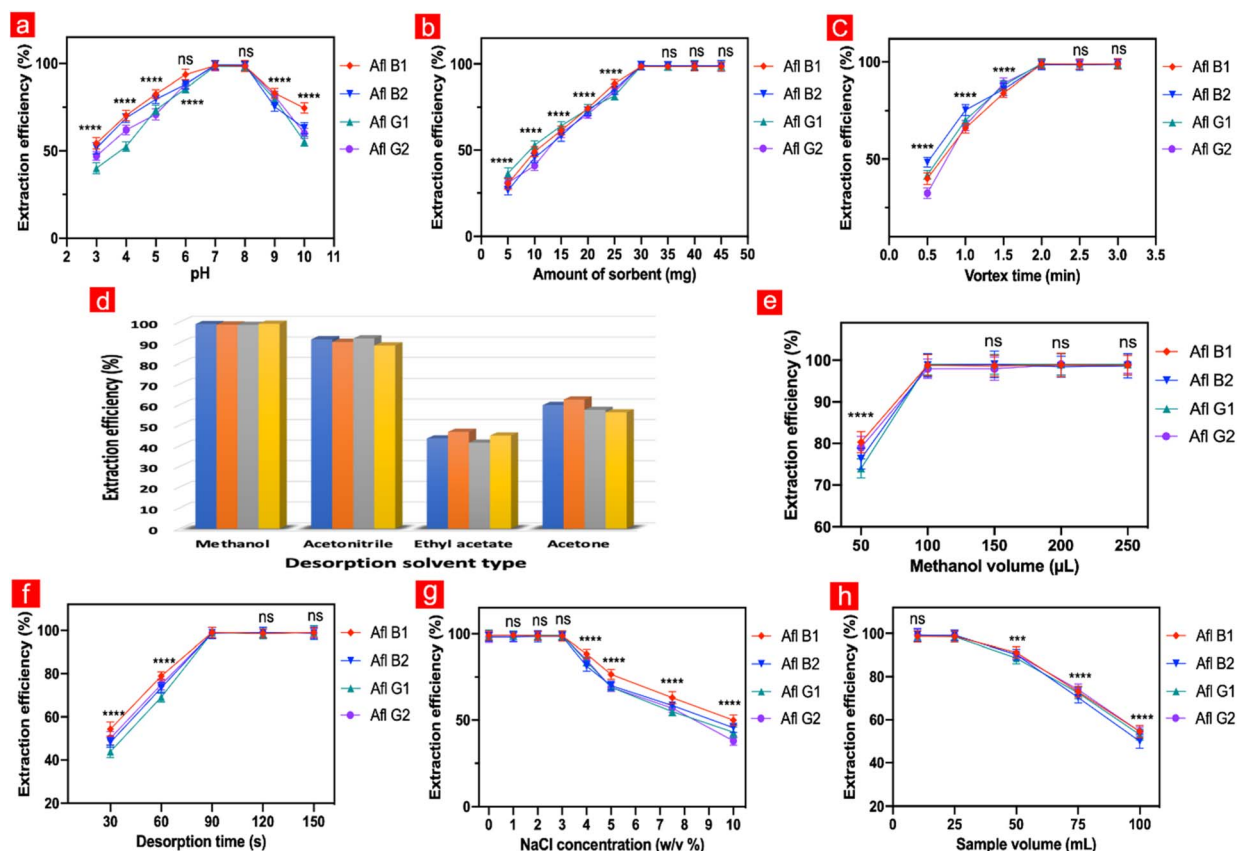


Fig. 2 The effect of influential parameters on the extraction efficiencies of aflatoxins: (a) pH, (b) amount of sorbent, (c) vortex time, (d) desorption solvent type, and (e) desorption solvent volume, (f) desorption time, (g) ionic strength, (h) sample volume; data are represented as mean  $\pm$  SD based on three independent experiments and significant differences between groups with (ns = not significant), \* ( $P < 0.05$ ), \*\* ( $P < 0.01$ ), \*\*\* ( $P < 0.001$ ), and \*\*\*\* ( $P < 0.0001$ ) using two-way ANOVA with Dunnett's multiple comparisons test, with individual variances computed for each comparison.



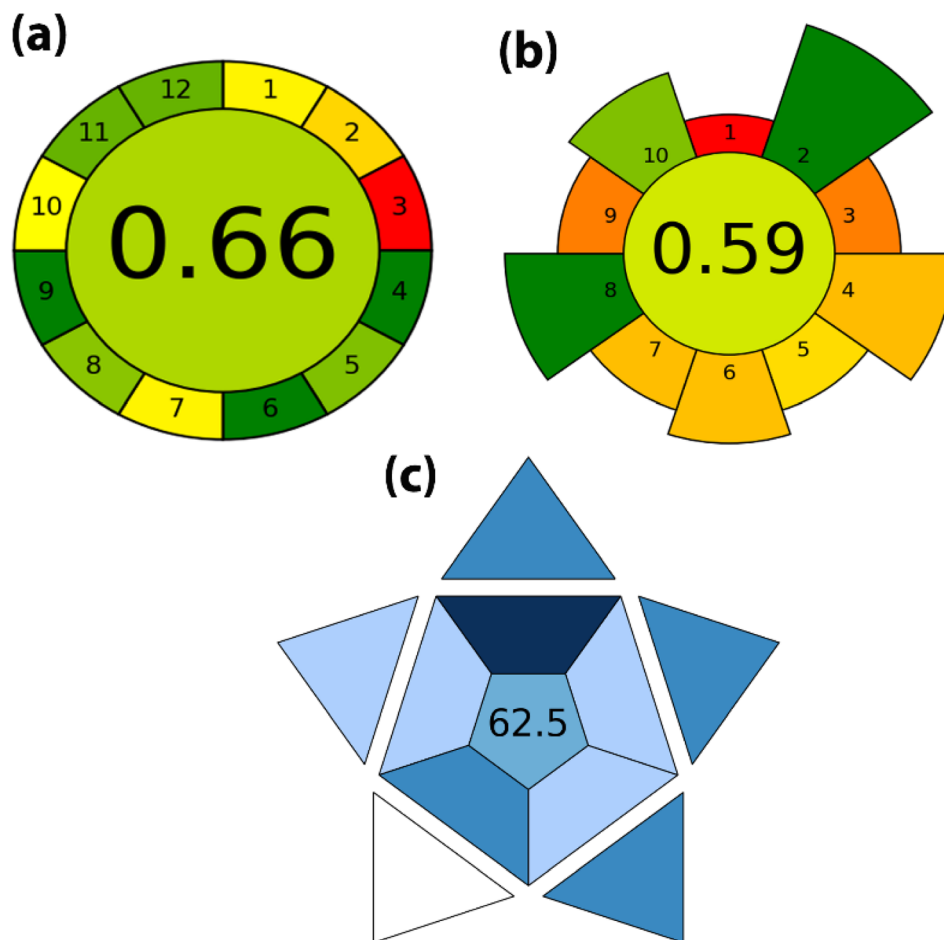


Fig. 3 The greenness evaluations of MCS/ZIF-L/KCDs -D $\mu$ SPE: (a) AGREE, (b) AGREEprep, (c) BAGI pictogram of the process.

and as indicated in Fig. 2(g), the extraction efficiencies were constant and maximum from 0–3% and then decreased. It can be concluded that by the augmentation of the concentration of salt, the viscosity of the solution increases, and the mass transfer of analytes from the solution to the surface of the sorbent decreases. Moreover, the salt molecules can occupy the active sites of the sorbent and lead to a decrease in extraction efficiencies.

Besides the desorption solvent volume, the volume of the sample solution also impacts the PF and should be precisely determined. Therefore, the sample volume in the range 10–100 mL was considered, and as indicated in Fig. 2(h), the extraction efficiencies were maximum and quantitative from 25 mL and then reduced. Hence, the sample volume of 25 mL was determined to be optimum.

### 3.3. Adsorbent reusability

The regenerability of MCS/ZIF-L/KCDs clarifies the potential and the efficiency of the sorbent. To this aim, the polluted adsorbent was mixed with 0.5 mL solution of methanol: acetonitrile (50 : 50 (v/v %)). The clean sorbent could be reused with extraction efficiencies over 98% and over 90% after four and six washings, respectively, which shows the high capability of MCS/ZIF-L/KCDs.

### 3.4. Statistical analysis

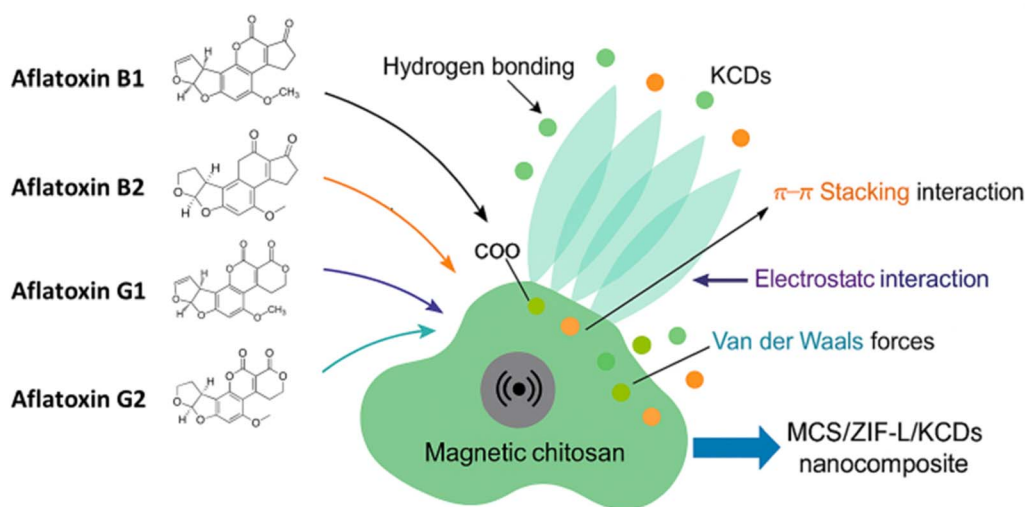
Statistical analysis was performed using GraphPad Prism 6 software (USA). Data were expressed as mean  $\pm$  standard deviation (SD). Two-way analysis of variance (ANOVA) followed by Dunnett's multiple comparison test was applied as a supportive statistical tool to compare the experimental conditions investigated during the optimization of the extraction procedure, including solution pH, sorbent amount (mg), NaCl concentration (w/v %), methanol volume ( $\mu$ L), vortex time (min), desorption time (s), and sample volume (mL). Statistical analysis was used only to confirm the observed trends in extraction efficiency, while the selection of the optimal conditions was primarily based on the highest extraction recovery and practical considerations.

### 3.5. Green evaluation metrics of the method

In recent years, several green metric tools have been developed to evaluate the environmental impact of analytical procedures.<sup>35</sup> The AGREE metric provides a visual and numerical assessment of analytical greenness based on the principles of green analytical chemistry, using a color scale from red to green with scores ranging from 0 to 1. The AGREE score obtained for the proposed MCS/ZIF-L/KCDs-MD- $\mu$ SPE method was 0.66,







Scheme 1 Schematic illustration of the proposed extraction mechanism of aflatoxins B1, B2, G1, and G2 using the MCS/ZIF-L/KCDs nanocomposite.

developed method. The detailed analytical performance results are presented in Table 1.

### 3.7. Extraction mechanism

The efficient extraction of aflatoxins B1, B2, G1, and G2 by the MCS/ZIF-L/KCDs nanocomposite can be attributed to the

synergistic contributions of the physical, chemical, and structural properties of the composite sorbent.<sup>36</sup> The hierarchical composite structure is designed to integrate the advantages of its individual components, namely MCS, ZIF-L nanosheets, and KCDs. The magnetic chitosan core provides a biocompatible and magnetically retrievable substrate containing abundant

Table 2 Application of MCS/ZIF-L/KCDs -D<sub>μ</sub>SPE for simultaneous separation and determination of aflatoxins B1, B2, G1, and G2 in different real samples

Sample	Spiked concentration (ng kg <sup>-1</sup> )				Found concentration (ng kg <sup>-1</sup> )				Relative recoveries (%)			
	B1	B2	G1	G2	B1	B2	G1	G2	B1	B2	G1	G2
Ziziphus jujube <sup>a</sup>	—	—	—	—	N.D.	N.D.	N.D.	N.D.	—	—	—	—
	10	10	10	10	9.5 <sup>b</sup> ± 0.3	9.8 ± 0.5	9.3 ± 0.6	9.4 ± 0.4	95.0	98.0	93.0	94.0
	50	50	50	50	49.3 ± 2.7	48.6 ± 2.6	49.0 ± 2.5	48.3 ± 3.0	98.6	97.2	98.0	96.6
	100	100	100	100	97.5 ± 3.1	95.3 ± 3.2	98.7 ± 2.9	96.5 ± 2.9	97.5	95.3	98.7	96.5
Wheat	—	—	—	—	N.D.	N.D.	N.D.	N.D.	—	—	—	—
	10	10	10	10	9.4 ± 0	9.5 ± 0.6	9.4 ± 0.2	9.6 ± 0.5	94.0	95.0	94.0	96.0
	50	50	50	50	48.2 ± 2.4	49.6 ± 3.2	47.5 ± 3.5	48.8 ± 2.3	96.4	99.2	95.0	97.6
	100	100	100	100	99.1 ± 2.4	96.6 ± 2.5	94.8 ± 2.3	95.1 ± 2.5	99.1 ± 2.7	96.6	94.8	95.1
Corn	—	—	—	—	N.D.	N.D.	N.D.	N.D.	—	—	—	—
	10	10	10	10	9.60 ± 0.5	9.90 ± 0.5	9.20 ± 0.4	9.70 ± 0.6	96.0	99.0	92.0	97.0
	50	50	50	50	49.1 ± 2.5	49.5 ± 2.2	47.6 ± 2.8	48.0 ± 3.5	98.2	99.0	95.2	96.0
	100	100	100	100	96.2 ± 2.8	98.9 ± 2.6	97.2 ± 3.3	98.5 ± 3.2	96.2	98.9	97.2	98.5
White rice	—	—	—	—	N.D.	N.D.	N.D.	N.D.	—	—	—	—
	10	10	10	10	9.10 ± 0.5	9.50 ± 0.4	9.30 ± 0.6	9.20 ± 0.5	91.0	95.0	93.0	92.0
	50	50	50	50	48.3 ± 2.3	48.6 ± 2.5	47.5 ± 2.6	49.1 ± 2.2	96.6	97.2	95.0	98.2
	100	100	100	100	98.6 ± 2.4	97.2 ± 3.2	97.8 ± 2.6	99.4 ± 2.1	98.6	97.2	97.8	99.4
Pistachio	—	—	—	—	N.D.	N.D.	N.D.	N.D.	—	—	—	—
	10	10	10	10	9.00 ± 0.6	9.40 ± 0.4	9.60 ± 0.5	9.30 ± 0.4	90.0	94.0	96.0	93.0
	50	50	50	50	47.6 ± 2.3	48.2 ± 2.0	46.5 ± 2.9	46.9 ± 2.5	95.2	96.4	93.0	93.8
	100	100	100	100	94.1 ± 3.0	96.8 ± 3.1	97.8 ± 2.6	96.2 ± 2.8	94.1	96.8	97.8	96.2
Walnut	—	—	—	—	N.D.	N.D.	N.D.	N.D.	—	—	—	—
	10	10	10	10	9.00 ± 0.3	9.30 ± 0.5	9.50 ± 0.6	9.10 ± 0.5	90.0	93.0	95.0	91.0
	50	50	50	50	48.3 ± 2.5	49.1 ± 2.1	48.5 ± 2.5	47.7 ± 2.2	96.6	98.2	97.0	95.4
	100	100	100	100	97.1 ± 3.1	98.6 ± 2.6	99.0 ± 2.2	98.5 ± 2.5	97.1	98.6	99.0	98.5

<sup>a</sup> Ziziphus jujube, wheat, corn, white rice, pistachios, and walnuts were all purchased from a local supermarket in Isfahan, Iran. <sup>b</sup> The obtained data are the mean of three replicates.



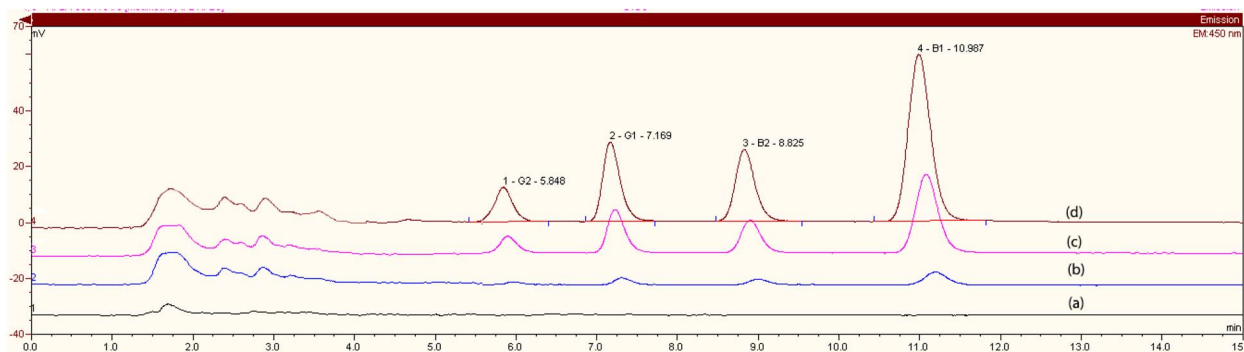


Fig. 4 HPLC-FLD chromatograms of aflatoxins B1, B2, G1, and G2 in ziziphus jujuba; (a) blank sample, and the spiked levels of (b) 10, (c) 50, and (d) 100 (ng kg<sup>-1</sup>) after applying the method.

hydroxyl and amine functional groups, which can participate in hydrogen bonding and polar interactions with aflatoxin molecules. These functional groups contribute to the affinity of the sorbent toward polar analytes while enabling convenient magnetic separation of the sorbent from the sample solution.

The ZIF-L nanosheets grown on the MCS surface introduce a porous leaf-like architecture with high surface accessibility and an increased surface area. This structure facilitates effective contact between the sorbent and the analytes, while the aromatic imidazole rings of ZIF-L can contribute to  $\pi$ - $\pi$  stacking interactions with the planar structures of aflatoxins. In addition, the nitrogen-containing framework of ZIF-L may promote dipole-related interactions with the aflatoxin molecules.

Furthermore, the incorporation of KCDs onto the MCS/ZIF-L composite surface provides additional active sites enriched with oxygen-containing functional groups such as -OH, -COOH, and C=O, as confirmed by FTIR and SEM-EDX analyses. These functional groups enhance the interaction between the sorbent and aflatoxin molecules through hydrogen bonding, dipole-dipole interactions, and van der Waals forces. The deposition of KCDs also increases the surface roughness and heterogeneity of the composite, which can contribute to improved analyte accessibility within the nanoscale structure.

The pH of the extraction medium plays an important role in the extraction efficiency. As discussed in Section 3.2, the extraction recoveries increased from pH 3 to 7, remained nearly constant between pH 7 and 8, and decreased at higher pH values. Therefore, PBS buffer solution (pH = 7.4) was selected as the optimal extraction medium. This observation is consistent with the experimentally determined pHPZC value of 7.3 for the MCS/ZIF-L/KCDs sorbent (Fig. S1), indicating that the sorbent surface is close to electrically neutral under near-neutral conditions. Such conditions favor effective interaction between the sorbent surface and aflatoxin molecules.

The rapid adsorption behavior observed during vortex-assisted extraction (optimal at 1.0 min) suggests that the hierarchical structure of the composite provides readily accessible active sites and facilitates fast mass transfer between the sorbent and analytes. After extraction, the magnetic core enables rapid separation of the sorbent from the sample

solution using an external magnet, eliminating the need for filtration or centrifugation. The bound aflatoxins can then be efficiently desorbed using methanol, whose polarity allows disruption of the sorbent-analyte interactions and ensures effective recovery of the target compounds.

As a result, the multifunctional and hierarchical architecture of the MCS/ZIF-L/KCDs nanocomposite provides multiple interaction pathways and a large accessible surface area, resulting in efficient extraction and preconcentration of aflatoxins from complex food matrices. The analytical merit of the proposed sorbent therefore arises from the synergistic integration of magnetic chitosan, ZIF-L, and KCDs in a single composite structure, making it a robust and versatile sorbent for the trace-level determination of aflatoxins in food samples (Scheme 1).

### 3.8. Application of the method

To consider the ability of the MCS/ZIF-L/KCDs-MD- $\mu$ SPE coupled with HPLC-FLD to be used in various matrices, simultaneous preconcentration/separation and determination of aflatoxins B1, B2, G1, and G2 was studied in ziziphus jujube, wheat, corn, white rice, pistachio, and walnut. To investigate the accuracy of the method, the concentrations of 50, 100, and 200 ng kg<sup>-1</sup> of aflatoxins B1, B2, G1, and G2 were spiked in ziziphus jujube. The relative recoveries (%) of 91.0–99.4 were obtained with RSDs (%)  $\leq$  3.5 ( $n = 3$ ). The results are indicated in Table 2. The ziziphus jujube HPLC chromatograms are revealed in Fig. 4.

### 3.9. Comparison of the proposed method

To evaluate the analytical performance of the proposed MCS/ZIF-L/KCDs-MD- $\mu$ SPE method, its figures of merit were compared with representative previously reported methods, as summarized in Table 3. Since the published methods differ in sorbent composition, extraction format, sample matrix, and validation conditions, the comparison should be considered descriptive rather than statistically inferential. Nevertheless, the proposed method exhibited low detection limits (0.002–0.003  $\mu$ g kg<sup>-1</sup>), satisfactory recoveries, and good precision (RSD  $\leq$  3.0%), demonstrating that it is analytically competitive and well



Table 3 Comparison of the proposed method with some recent studies for the simultaneous extraction and determination of aflatoxin B1, B2, G1, and G2 in foodstuffs

Method	Adsorbent	Sorbent amount (mg)	Matrix complexity	Detection technique	LDR ( $\mu\text{g kg}^{-1}$ )	LOD ( $\mu\text{g kg}^{-1}$ )	RSD (%)	Extraction time (min)	Reusability	Ref.
MD- $\mu\text{SPE}$	MCS/ZIF-L/KCDs nanocomposites	25.0	Ziziphus jujube, wheat, corn, white rice, pistachio, walnut	HPLC-FLD	0.01–1000	0.002–0.003	$\leq 3.0$	1.0	6.0	This study
MD- $\mu\text{SPE}$	Sp-M-Dpi <sup>a</sup>	150	Pistachio	HPLC-FLD	2.0–10.0	0.02–0.07	<5.4	1.0	—	37
MD- $\mu\text{SPE}$	Dummy template MIP	55.0	Nuts, grains	HPLC-FLD	0.15–100	0.059–0.208	<5.4	<35	8.0	38
SPE	Activated carbon-boron	5.0	Pistachio, walnut, cashew, nut	HPLC-FLD	0.12–0.10	0.04–0.16	<7.0	3.0	10.0	39
MSPE	Fe <sub>3</sub> O <sub>4</sub> @SiO <sub>2</sub> @TiO <sub>2</sub> APTMS-CFA	10.0	Hazelnut, peanut, almond	HPLC-FLD	0.09–12.0	0.05–0.13	<7.1	4.0	8.0	40
SPE	Skeleton of polystyrene-polyvinyl pyrrolidone nanofibers	20.0	Plant- and animal-based food samples	HPLC-FLD	0.5–5.0	0.07–0.17	<8.0	5.0	—	41

<sup>a</sup> Sp-M-Dp: polydopamine-coated magnetic spirulina nanocomposite.

suitable for the separation, preconcentration, and determination of aflatoxins in complex food matrices.

## 4. Conclusion

In this study, a novel MCS/ZIF-L/KCDs granular-leaf hybrid nanocomposite was successfully synthesized and applied as an efficient sorbent for MD- $\mu\text{SPE}$  of aflatoxins B1, B2, G1, and G2 from ziziphus jujube, wheat, corn, white rice, pistachio, and walnut samples before HPLC-FLD determination. The developed method exhibited several advantages, including low consumption of organic solvents and sorbents, rapid extraction, and simple operation. Green analytical chemistry evaluation using AGREE, AGREEprep, and BAGI confirmed the environmentally friendly nature of the proposed procedure. Furthermore, the method demonstrated satisfactory analytical performance, including wide linear ranges, acceptable precision, and low detection limits. The obtained results indicate that the MCS/ZIF-L/KCDs-based MD- $\mu\text{SPE}$  coupled with HPLC-FLD provides a reliable, sensitive, and environmentally friendly strategy for the separation, preconcentration, and determination of aflatoxins in grain and nut samples. Therefore, the developed method shows strong potential for application in routine food safety monitoring and quality control of mycotoxin contamination.

## Conflicts of interest

The authors declare no conflict of interest.

## Data availability

Due to the University legal confidentiality requirements, the data can not be available.

## Acknowledgements

The authors gratefully appreciate the University of Jiroft and Erciyes University for their valuable support of this research study.

## References

- 1 F. Moghadasi, S. Roudbarmohammadi, S. Amanloo, F. Nikoomanesh and M. Roudbary, *Mol. Biol. Rep.*, 2024, **51**, 53.
- 2 B. Balan, A. S. Dhaulaniya, M. Kumar, M. Kumar and P. Kumar, *Food Saf. Health*, 2024, **2**, 39–71.
- 3 H. F. Hassan, K. Zgheib, C. F. Iskandar, A. Chalak, N. Alwan and M. G. Abiad, *Sci. Rep.*, 2024, **14**, 25761.
- 4 A. Jallow, H. Xie, X. Tang, Z. Qi and P. Li, *Compr. Rev. Food Sci. Food Saf.*, 2021, **20**, 2332–2381.
- 5 A. Kumar, H. Pathak, S. Bhadauria and J. Sudan, *Food Prod., Process. Nutr.*, 2021, **3**, 17.
- 6 V. Navale, K. R. Vamkudoth, S. Ajmera and V. Dhuri, *Toxicol Rep.*, 2021, **8**, 1008–1030.



- 7 K. Mukhtar, B. G. Nabi, S. Ansar, Z. F. Bhat, R. M. Aadil and A. Mousavi Khaneghah, *Toxicon*, 2023, **232**, 107227.
- 8 K. Zhang, B. Flannery and L. Zhang, *J. Agric. Food Chem.*, 2024, **72**, 8380–8388.
- 9 M. Carvajal-Moreno, *J. Cereal Sci.*, 2022, **103**, 103293.
- 10 L. Shi, A. Li, Y. Xu, H. Yang and G. Yang, *Microchim. Acta*, 2025, **192**, 307.
- 11 A. Castell, N. Arroyo-Manzanares, P. Viñas, I. López-García and N. Campillo, *TrAC, Trends Anal. Chem.*, 2024, **178**, 117826.
- 12 M. Shirani, S. Sepahi, O. Ozalp and M. Soylak, *Int. Dairy J.*, 2025, **165**, 106210.
- 13 M. Shirani, F. Ansari, M. Shabanian, U. Wagenknecht, Q. Salamat, M. Faraji, M. Basij and M. Adeli, *Microchem. J.*, 2024, **205**, 111254.
- 14 J. Wei, P. Fan, Y. Huang, H. Zeng, R. Jiang, Z. Wu, Y. Zhang and Z. Hu, *Org. Chem. Front.*, 2024, **11**, 3459–3464.
- 15 M. Soylak, S. Sajjad, Q. Salamat and H. E. H. Ahmed, *Food Chem.*, 2025, **490**, 145101.
- 16 S. Lu, Y.-J. Zhang, Y.-J. Cheng, Z.-H. Qin, G.-D. Wang, Y. Bai, Y. Lin, H. Wang, Y. Sui, L. Hou and Y.-Z. Li, *J. Mater. Chem. A*, 2025, **13**, 10581–10589.
- 17 S. N. Pandey, M. Afzal, A. Goyal, G. Padma Priya, B. Mohanty, K. Goyal, M. Rana and M. Imran, *Inorg. Chem. Commun.*, 2025, **179**, 114671.
- 18 S. Wang, L. Luo, A. Wu, D. Wang, L. Wang, Y. Jiao and C. Tian, *Coord. Chem. Rev.*, 2024, **498**, 215464.
- 19 M. Maneesha, P. C. Preethi, A. Harisankar, T. G. Sreeja, V. K. Ratheesh Kumar, S. T. Veedu and R. Raghunandan, *Microchem. J.*, 2025, **210**, 113046.
- 20 L. Gao, H. Yang, Y. Lu, S. Chen, L. He and J. Liu, *Food Chem.*, 2024, **458**, 140215.
- 21 L. Gao, Y. Lu, H. Yang, L. Guo, S. Chen and J. Liu, *Microchem. J.*, 2025, **210**, 112961.
- 22 M. Ghorbani, M. Keshavarzi, M. Pakseresht, P. Mohammadi, A. Shams, A. Mehraban and A. Ismailzadeh, *Anal. Bioanal. Chem.*, 2023, **415**, 5681–5694.
- 23 G. Khalilipour, A. R. Karamibonari, M. Movassaghghazani, J. Shayegh and M. R. Afshar Mogaddam, *Microchem. J.*, 2024, **202**, 110806.
- 24 R. Atchudan, T. N. J. I. Edison, S. Perumal, R. Vinodh, A. K. Sundramoorthy, R. S. Babu and Y. R. Lee, *Chemosensors*, 2021, **9**, 166.
- 25 M. Shirani, A. Aslani, F. Ansari, E. Parandi, H. R. Nodeh and E. Jahanmard, *Microchem. J.*, 2023, **189**, 108507.
- 26 R. Moradi, M. Seraji, N. P. Khalili, Q. Salamat and M. Soylak, in *Fundamentals and Biomedical Applications of Chitosan Nanoparticles*, Elsevier, 2025, pp. 447–496.
- 27 C. J. Wijaya, S. Ismadji, H. W. Apamarta and S. Gunawan, *Molecules*, 2021, **26**, 4416.
- 28 J. He, Y. Xiong, H. Mu, P. Li, Y. Deng, W. Zou and Q. Zhao, *Crystals*, 2023, **13**, 564.
- 29 H. Li, Y. Cheng, J. Li, T. Li, J. Zhu, W. Deng, J. Zhu and D. He, *Nanomaterials*, 2022, **12**, 4008.
- 30 X. Li, D. Zeng, Z. He, P. Ke, Y. Tian and G. Wang, *Carbohydr. Polym.*, 2022, **276**, 118729.
- 31 M. Aslan and H. Eskalen, *Fullerenes, Nanotubes Carbon Nanostruct.*, 2021, **29**, 1026–1033.
- 32 M. Xie, L. Zeng, Q. Zhang, Y. Kang, H. Xiao, Y. Peng, X. Chen and J. Luo, *J. Alloys Compd.*, 2015, **647**, 892–905.
- 33 K. S. Park, Z. Ni, A. P. Côté, J. Y. Choi, R. Huang, F. J. Uribe-Romo, H. K. Chae, M. O'Keeffe and O. M. Yaghi, *Proc. Natl. Acad. Sci. U. S. A.*, 2006, **103**, 10186–10191.
- 34 H. Li, Y. Zhang, S. Li, J. Shi, H. Wu, A. Jabbarzadeh, J. Liu, T. Cao, X. Fan and F. Zhou, *Carbon N. Y.*, 2026, **246**, 120869.
- 35 M. Shirani, Q. Salamat, M. Amirani Poor, H. M. Nejad and M. Soylak, *J. Food Compos. Anal.*, 2025, **142**, 107388.
- 36 Q. Long, H. Zhao, T. Qiu, H. Wu, H. Yan and S. Qiu, *Colloids Surf., A*, 2025, **727**, 138247.
- 37 R. Karami-Osboo, F. Ahmadpoor, M. Nasrollahzadeh and M. Maham, *Food Chem.*, 2022, **377**, 131967.
- 38 R. Thati, B. S. Seetha, P. Alegete and M. K. R. Mudiam, *Food Chem.*, 2024, **433**, 137342.
- 39 H. S. Karapınar and A. Balıkçioğlu, *J. Food Compos. Anal.*, 2022, **112**, 104680.
- 40 H. S. Karapınar and A. Bilgiç, *J. Food Compos. Anal.*, 2022, **105**, 104261.
- 41 Y. Wang, L. Chu, J. Qu, B. Ding and X. Kang, *Food Chem.*, 2024, **436**, 137699.

